TLM Extension to Electromagnetic Field Analysis of Anisotropic and Dispersive Media: A Unified Field Equation

Arij Farhat, Sandrick Le Maguer, Patrick Queffelec, Michel Ney

TLM Extension to Electromagnetic Field Analysis of Anisotropic and Dispersive Media: A Unified Field Equation

Arij Léo Farhat, Sandrick Le Maguer, Patrick Quéffélec, and Michel Ney

***Abstract*—The transmission-line matrix (TLM) method, in time domain, is extended to account for the presence of anisotropic and dispersive media in electromagnetic structures or devices. The model is thoroughly constructed by using Maxwell's equations that make it a unified general TLM formulation. Numerical results are compared with experimental measurements; hence, in the case of ferrite-based structures, validating the model and showing the accuracy of the approach.**

***Index Terms*—Anisotropic and dispersive media, ferrites, nonreciprocal circuits, permeability, time-domain analysis, transmission-line matrix (TLM) method.**

I. Introduction

OVER THE last few years, the rapid development of communication applications has generated a growing interest for miniaturization and cost reduction of microwave devices. The increase of operating frequencies and tunability are additional constraints that require more complex and accurate models for computer-aided design (CAD) of communication system components.

Among those components, circulators and isolators use the anisotropic properties of ferrite materials to insure the required nonreciprocal character of the wave propagation. Their field-dependent permeability provides some tunability of circuits, such as filters and phase shifters. More recently, their high refractive index has found interest in the size reduction of patch antennas. It has been demonstrated that antennas with a magneto-dielectric substrate that exhibits a permeability greater than its permittivity has better performances than those deposited on pure dielectric substrates [1].

To assist the design of ferrite-based microwave devices, one needs to have a proper design tool enabling the prediction of the microwave behavior of ferrite samples whatever their magnetization state. For instance, it is considered to use hexaferrite materials that operate at the remanent state to work out self-biased circulators [2]. It would also be very interesting to be able to predict the variation of the performances of patch antennas deposited on a ferrite substrate as a function of its magnetization state.

Magnetized ferrites are anisotropic media. Their electromagnetic properties must be represented by a tensor quantity, called the permeability tensor. The usual permeability model based on the Polder formulations [3] is only valid for a saturated sample. Designing ferrite microwave devices requires the knowledge of the permeability tensor $\overleftrightarrow{\mu}$ of the magnetic materials used as a substrate, which directly influence the guided wavelengths and the performances of the devices.

The objective of this paper is twofold: first, to develop a rigorous model for field computation in the presence of complex media and second to insert a new model of nonsaturated ferrites [4] into the algorithm.

Presently there is no commercial simulator capable to account for the complex physical phenomena appearing in the electromagnetic structures using magnetized magnetic materials, such as the following:

- nonhomogenous internal polarization field implying a space variation of the permeability;
- nonsaturated zones in plate ferrite samples due to demagnetizing fields even for substrates biased with a strong dc field;
- dynamic interactions between magnetic domains in nonsaturated regions of the ferrite substrate and between grains whatever the magnetization state;
- magnetostatic modes.

The above phenomena must be accounted for in the model, as they strongly affect the performances of the device in terms of bandwidth, insertion losses, etc. They can also preclude miniaturization of circulators. We have observed that a cutoff band appeared in the experimental response of miniaturized Y-junction circulators [5]. This degradation was missing in the transmission signal predicted by commercial softwares.

Finally, the time-domain character of the TLM not only allows a wideband characterization, but also accounts for the presence of potential nonlinearities.

To predict the dynamic behavior of polycrystalline ferrites for an arbitrary magnetization state, one proposes a theoretical approach that provides all tensor components. They are functions of the dc bias field strength and direction, the sample geometry,

A. L. Farhat is with Cobham Microwaves, 91978 Villebon-sur-Yvette, France (e-mail: arij.farhat@telecom-bretagne.eu).

S. Le Maguer is with "Sprezzatura," 29200 Brest, France (e-mail: Sandrickl@emaguer.com).

P. Quéffélec is with the Laboratoire des Sciences et Techniques de l'Information, Communication et de la Connaissance (Lab-STICC, UMR CNRS), Université de Bretagne Occidentale, UFR Sciences, 29200 Brest, France (e-mail: patrick.queffelec@univ-brest.fr).

M. Ney is with the Laboratoire des Sciences et Techniques de l'Information, Communication et de la Connaissance (Lab-STICC, UMR CNRS), Telecom Bretagne, 29200 Brest, France (e-mail: michel.ney@telecom-bretagne.eu).

and static magnetic characteristics such as saturation magnetization and magnetocrystalline anisotropy field. Finally, sample structural properties (magnetic domains and grains shape) are accounted for by the model. Details of the proposed theoretical approach can be found in [4].

In this paper, the TLM is first extended to general dispersive and anisotropic media. Some pioneer work, based on circuit analogy, was presented for the TLM model [6]–[8]. This paper focuses on a formulation based directly on Maxwell's equations [9]. It gives a clear and systematic derivation that constitutes a general approach, which can be applied to any type of media. Two different types of media are then studied: unmagnetized plasma considered as a dispersive medium and a nonsaturated ferrite (with an arbitrary magnetization state).

II. TLM Theoretical Model

A. Formulation: Unified Field Equation

Let us consider a general anisotropic and dispersive medium in which electromagnetic quantities are governed by the general Maxwell curl equations in time domain

$$\begin{aligned}\begin{bmatrix} \nabla \times \vec{H} \\ -\nabla \times \vec{E} \end{bmatrix} - \begin{bmatrix} \vec{J}_{ef} \\ \vec{J}_{mf} \end{bmatrix} &= \frac{\partial}{\partial t} \begin{bmatrix} \varepsilon_0 \vec{E} \\ \mu_0 \vec{H} \end{bmatrix} + \begin{bmatrix} \underline{\underline{\sigma_e}} * \vec{E} \\ \underline{\underline{\sigma_m}} * \vec{H} \end{bmatrix} \\ &\quad + \frac{\partial}{\partial t} \begin{bmatrix} \varepsilon_0 \underline{\underline{\chi_e}} & \underline{\underline{\xi_r}}/c_0 \\ \underline{\underline{\zeta_r}}/c_0 & \mu_0 \underline{\underline{\chi_m}} \end{bmatrix} * \begin{bmatrix} \vec{E} \\ \vec{H} \end{bmatrix} \end{aligned} \tag{1}$$

where subscript e and m stand for electric and magnetic, respectively, * denotes the convolution operation, double underlined quantities are tensors, c_0 is the speed of light in vacuum, and the other electromagnetic quantities are defined in Table I.

For the symmetrical condensed node (SCN) TLM, the presence of materials affects the field values at the node center, while arm impedances are all kept at free-space value. The application of the general procedure described by Peña and Ney in [9] for general media is new and not straightforward. However, it has the advantage to allow the development for all TLM nodes such as hybrid symmetrical condensed node (HSCN) or super condensed symmetrical condensed node (SSCN) nodes, by following the same general procedure.

TABLE I
Electromagnetic Quantities

Quantity	Symbol	Units
Electric field	E	V m^{-1}
Magnetic field	H	A m^{-1}
Electric current density	J_e	A m^{-2}
Magnetic voltage density	J_m	V m^{-2}
Electric flux density	D	C m^{-2}
Magnetic flux density	B	Wb m^{-2}
Free electric current density	J_{ef}	A m^{-2}
Free magnetic voltage density	J_{mf}	V m^{-2}
Magnetization	M ou 4πM	T (ou Oe ??)
Electric susceptibility	χ_e	
Magnetic susceptibility	χ_m	
Electric conductivity	σ_e	S m^{-1}
Magnetic resistivity	σ_m	Ω m^{-1}
Relative permeability	μ	
Relative permittivity	ε	

Equation (1) can be written as (2), shown at the bottom of this page.

1) Maxwell–Ampere: Consider the x-component of the Maxwell–Ampere's curl equation in (2),

$$\begin{aligned}\frac{\partial H_z}{\partial y} - \frac{\partial H_y}{\partial z} - J_{ex} &= \varepsilon_0 \frac{\partial E_x}{\partial t} \\ &\quad + (\sigma_e^{xx} * E_x + \sigma_e^{xy} * E_y + \sigma_e^{xz} * E_z) \\ &\quad + \frac{\partial}{\partial t} [\varepsilon_0 (\chi_e^{xx} * E_x + \chi_e^{xy} * E_y + \chi_e^{xz} * E_z) \\ &\qquad + \xi_r^{xx} * H_x + \xi_r^{xy} * H_y + \xi_r^{xz} * H_z] . \end{aligned} \tag{3}$$

$$\begin{bmatrix} \frac{\partial H_z}{\partial y} - \frac{\partial H_y}{\partial z} \\ \frac{\partial H_x}{\partial z} - \frac{\partial H_z}{\partial x} \\ \frac{\partial H_y}{\partial x} - \frac{\partial H_x}{\partial y} \\ -\frac{\partial E_z}{\partial y} + \frac{\partial E_y}{\partial z} \\ -\frac{\partial E_x}{\partial z} + \frac{\partial E_z}{\partial x} \\ -\frac{\partial E_y}{\partial x} + \frac{\partial E_x}{\partial y} \end{bmatrix} - \begin{bmatrix} J_{ex} \\ J_{ey} \\ J_{ez} \\ J_{mx} \\ J_{my} \\ J_{mz} \end{bmatrix} = \frac{\partial}{\partial t} \begin{bmatrix} \varepsilon_0 E_x \\ \varepsilon_0 E_y \\ \varepsilon_0 E_z \\ \mu_0 H_x \\ \mu_0 H_y \\ \mu_0 H_z \end{bmatrix} + \begin{bmatrix} \sigma_e^{xx} & \sigma_e^{xy} & \sigma_e^{xz} & & 0 & \\ \sigma_e^{yx} & \sigma_e^{yy} & \sigma_e^{yz} & & & \\ \sigma_e^{zx} & \sigma_e^{zy} & \sigma_e^{zz} & & & \\ & 0 & & \sigma_m^{xx} & \sigma_m^{xy} & \sigma_m^{xz} \\ & & & \sigma_m^{yx} & \sigma_m^{yy} & \sigma_m^{yz} \\ & & & \sigma_m^{zx} & \sigma_m^{zy} & \sigma_m^{zz} \end{bmatrix} * \begin{bmatrix} E_x \\ E_y \\ E_z \\ H_x \\ H_y \\ H_z \end{bmatrix}$$

$$+ \frac{\partial}{\partial t} \begin{bmatrix} \varepsilon_0 \chi_e^{xx} & \varepsilon_0 \chi_e^{xy} & \varepsilon_0 \chi_e^{xz} & \xi_r^{xx}/c_0 & \xi_r^{xy}/c_0 & \xi_r^{xz}/c_0 \\ \varepsilon_0 \chi_e^{yx} & \varepsilon_0 \chi_e^{yy} & \varepsilon_0 \chi_e^{yz} & \xi_r^{yx}/c_0 & \xi_r^{yy}/c_0 & \xi_r^{yz}/c_0 \\ \varepsilon_0 \chi_e^{zx} & \varepsilon_0 \chi_e^{zy} & \varepsilon_0 \chi_e^{zz} & \xi_r^{zx}/c_0 & \xi_r^{zy}/c_0 & \xi_r^{zz}/c_0 \\ \zeta_r^{xx}/c_0 & \zeta_r^{xy}/c_0 & \zeta_r^{xz}/c_0 & \mu_0 \chi_m^{xx} & \mu_0 \chi_m^{xy} & \mu_0 \chi_m^{xz} \\ \zeta_r^{yx}/c_0 & \zeta_r^{yy}/c_0 & \zeta_r^{yz}/c_0 & \mu_0 \chi_m^{yx} & \mu_0 \chi_m^{yy} & \mu_0 \chi_m^{yz} \\ \zeta_r^{zx}/c_0 & \zeta_r^{zy}/c_0 & \zeta_r^{zz}/c_0 & \mu_0 \chi_m^{zx} & \mu_0 \chi_m^{zy} & \mu_0 \chi_m^{zz} \end{bmatrix} * \begin{bmatrix} E_x \\ E_y \\ E_z \\ H_x \\ H_y \\ H_z \end{bmatrix} \tag{2}$$

The above relation can be sampled in the plane yOz, according to the illustration shown in Fig. 1, and shown in (4) at the bottom of this page.

By multiplying this equation by $Z_0\Delta y\Delta z$, one can write (5), shown at the bottom of this page.

Rearranging (5) yields (6), shown at the bottom of this page.

Now, by setting

$$\hat{Y}_{sx} + 4 = \frac{2}{\bar{C}_x} \text{ and } \bar{C}_x = \frac{s\Delta x}{2\Delta y\Delta z} \tag{7}$$

with $s = 2c_0\Delta t$ and

$$\tilde{E}_x = \frac{E_1^x + E_{12}^x + E_2^x + E_9^x + \hat{Y}_{sx}E_{13}^x}{4 + \hat{Y}_{sx}}. \tag{8}$$

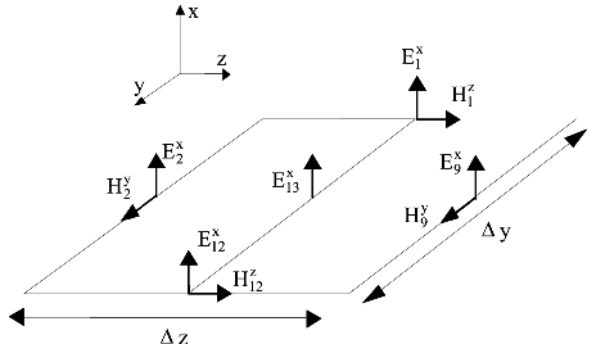

Fig. 1. Field component sampling for discretization of Maxwell–Ampere's curl's equation x-component.

Equation (6) becomes (9), shown at the bottom of the following page. Now, one can introduce the incident arm voltage

$$\begin{aligned}
&\left[\frac{(H_{12}^z - H_1^z)}{\Delta y} + \frac{(H_2^y - H_9^y)}{\Delta z}\right]^{(n-1/2)} \\
&\quad = \frac{2}{Z_0c_0\Delta x\Delta t}\Delta x\left[E_x^{(n)} - \tilde{E}_x^{(n-1/2)}\right] \\
&\qquad + \left(\frac{\sigma_e^{xx}}{\Delta x} * \Delta x E_x^{(n)} + \frac{\sigma_e^{xy}}{\Delta y} * \Delta y E_y^{(n)} + \frac{\sigma_e^{xz}}{\Delta z} * \Delta z E_z^{(n)}\right) + J_{ex}^{(n)} \\
&\qquad + \frac{1}{Z_0c_0}\frac{\partial}{\partial t}\left[\begin{array}{l}\left(\frac{\chi_e^{xx}}{\Delta x} * \Delta x E_x^{(n)} + \frac{\chi_e^{xy}}{\Delta y} * \Delta y E_y^{(n)} + \frac{\chi_e^{xz}}{\Delta z} * \Delta z E_z^{(n)}\right) \\ + \left(\frac{\xi_r^{xx}}{\Delta x} * Z_0\Delta x H_x^{(n)} + \frac{\xi_r^{xy}}{\Delta y} * Z_0\Delta y H_y^{(n)}\right. \\ \qquad\qquad \left. + \frac{\xi_r^{xz}}{\Delta z} * Z_0\Delta z H_z^{(n)}\right)\end{array}\right]
\end{aligned} \tag{4}$$

$$\begin{aligned}
&[Z_0\Delta z\,(H_{12}^z - H_1^z) + Z_0\Delta y\,(H_2^y - H_9^y)]^{(n-1/2)} \\
&\quad = \frac{2\Delta y\Delta z}{c_0\Delta x\Delta t}\Delta x\left[E_x^{(n)} - \tilde{E}_x^{(n-1/2)}\right] \\
&\qquad + Z_0\Delta y\Delta z\left(\frac{\sigma_e^{xx}}{\Delta x} * \Delta x E_x^{(n)} + \frac{\sigma_e^{xy}}{\Delta y} * \Delta y E_y^{(n)} + \frac{\sigma_e^{xz}}{\Delta z} * \Delta z E_z^{(n)}\right) + Z_0\Delta y\Delta z J_{ex}^{(n)} \\
&\qquad + \frac{\Delta y\Delta z}{c_0}\frac{\partial}{\partial t}\left[\begin{array}{l}\left(\frac{\chi_e^{xx}}{\Delta x} * \Delta x E_x^{(n)} + \frac{\chi_e^{xy}}{\Delta y} * \Delta y E_y^{(n)} + \frac{\chi_e^{xz}}{\Delta z} * \Delta z E_z^{(n)}\right) \\ + \left(\frac{\xi_r^{xx}}{\Delta x} * Z_0\Delta x H_x^{(n)} + \frac{\xi_r^{xy}}{\Delta y} * Z_0\Delta y H_y^{(n)} + \frac{\xi_r^{xz}}{\Delta z} * Z_0\Delta z H_z^{(n)}\right)\end{array}\right]
\end{aligned} \tag{5}$$

$$\begin{aligned}
&[Z_0\Delta z\,(H_{12}^z - H_1^z) + Z_0\Delta y\,(H_2^y - H_9^y)]^{(n-1/2)} \\
&\quad = \frac{4\Delta y\Delta z}{2c_0\Delta x\Delta t}\Delta x\left[E_x^{(n)} - \tilde{E}_x^{(n-1/2)}\right] \\
&\qquad + Z_0\frac{\Delta y\Delta z}{\Delta x}\left(\frac{\Delta x\sigma_e^{xx}}{\Delta x} * \Delta x E_x^{(n)} + \frac{\Delta x\sigma_e^{xy}}{\Delta y} * \Delta y E_y^{(n)} + \frac{\Delta x\sigma_e^{xz}}{\Delta z} * \Delta z E_z^{(n)}\right) + Z_0\frac{\Delta y\Delta z}{\Delta x}\Delta x J_{ex}^{(n)} \\
&\qquad + 2\Delta t\frac{\Delta y\Delta z}{2c_0\Delta t\Delta x}\frac{\partial}{\partial t}\left[\begin{array}{l}\left(\frac{\Delta x\chi_e^{xx}}{\Delta x} * \Delta x E_x^{(n)} + \frac{\Delta x\chi_e^{xy}}{\Delta y} * \Delta y E_y^{(n)} + \frac{\Delta x\chi_e^{xz}}{\Delta z} * \Delta z E_z^{(n)}\right) \\ + \left(\frac{\Delta x\xi_r^{xx}}{\Delta x} * Z_0\Delta x H_x^{(n)} + \frac{\Delta x\xi_r^{xy}}{\Delta y} * Z_0\Delta y H_y^{(n)} + \frac{\Delta x\xi_r^{xz}}{\Delta z} * Z_0\Delta z H_z^{(n)}\right)\end{array}\right]
\end{aligned} \tag{6}$$

a_i at time $n-1/2$ and link them to field components at the node center and at time n,

$$\begin{aligned}
&\bar{C}_x(a_1+a_{12}+a_2+a_9)^{(n-1/2)} \\
&\quad = \Delta x E_x^{(n)} + Z_0 \frac{\bar{C}_x}{2}\frac{\Delta y \Delta z}{\Delta x} \\
&\qquad \times \left(\frac{\Delta x \sigma_e^{xx}}{\Delta x} * \Delta x E_x^{(n)} + \frac{\Delta x \sigma_e^{xy}}{\Delta y} * \Delta y E_y^{(n)} \right. \\
&\qquad\quad \left. + \frac{\Delta x \sigma_e^{xz}}{\Delta z} * \Delta z E_z^{(n)} \right) + Z_0 \frac{\bar{C}_x}{2}\frac{\Delta y \Delta z}{\Delta x} \Delta x J_{ex}^{(n)} \\
&\qquad + \frac{\Delta t}{2}\frac{\partial}{\partial t}\left[\left(\frac{\Delta x \chi_e^{xx}}{\Delta x} * \Delta x E_x^{(n)} + \frac{\Delta x \chi_e^{xy}}{\Delta y} \right.\right. \\
&\qquad\qquad * \Delta y E_y^{(n)} + \left.\frac{\Delta x \chi_e^{xz}}{\Delta z} * \Delta z E_z^{(n)} \right) \\
&\qquad\qquad + \left(\frac{\Delta x \xi_r^{xx}}{\Delta x} * Z_0 \Delta x H_x^{(n)} + \frac{\Delta x \xi_r^{xy}}{\Delta y} \right. \\
&\qquad\qquad \left.\left. * Z_0 \Delta y H_y^{(n)} + \frac{\Delta x \xi_r^{xz}}{\Delta z} * Z_0 \Delta z H_z^{(n)} \right) \right] \qquad (10)
\end{aligned}$$

by setting

$$\begin{aligned}
\bar{\sigma}_e^{ij} &= Z_0 \Delta k \bar{C}_i \sigma_e^{ij}, \qquad i \neq j \\
\bar{\sigma}_e^{ii} &= Z_0 \frac{\Delta j \Delta k}{\Delta i} \bar{C}_i \sigma_e^{ii}, \qquad i = j \qquad (11) \\
\bar{\chi}_e^{ij} &= \frac{\Delta t \Delta i}{2 \Delta j} \chi_e^{ij} \text{ and } \bar{\xi}_r^{ij} = \frac{\Delta t \Delta i}{2 \Delta j} \xi_r^{ij} \qquad (12)
\end{aligned}$$

$$\begin{cases}
\left[\Delta x E_x^{(n)}\right]_{\text{source}} = -\frac{Z_0}{2}\bar{C}_x \frac{\Delta y \Delta z}{\Delta x} \Delta x J_{ex}^{(n)} \\
\left[\Delta x E_x^{(n)}\right]_{\text{nor}} = \bar{C}_x \left(a_1 + a_{12} + a_2 + a_9\right)^{(n-1/2)} \\
\left[\Delta x E_x^{(n)}\right]_{\text{nor}} + \left[\Delta x E_x^{(n)}\right]_{\text{source}} = \left[\Delta x E_x^{(n)}\right]_r .
\end{cases} \qquad (13)$$

The subscript nor indicates field components computed from incident voltages a_i, source is the excitation that can exist at the note location and r is the resulting field at the node center.

Equation (13) yields (14), shown at the bottom of this page.

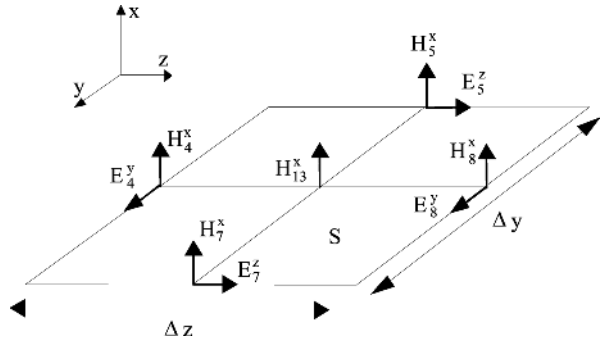

Fig. 2. Field component sampling for discretization of Maxwell–Faraday's curl's equation x-component.

Convolution products can be eliminated via Laplace transform and (14) can be written in the compact form

$$\begin{aligned}
&[\Delta x E_x]_r \\
&\quad = \left(1 + \bar{\sigma}_e^{xx} + s\bar{\chi}_e^{xx}\right)\Delta x E_x + \left(\bar{\sigma}_e^{xy} + s\bar{\chi}_e^{xy}\right)\Delta y E_y \\
&\qquad + \left(\bar{\sigma}_e^{xz} + s\bar{\chi}_e^{xz}\right)\Delta z E_z + s\bar{\xi}_r^{xx} Z_0 \Delta x H_x \\
&\qquad + s\bar{\xi}_r^{xy} Z_0 \Delta y H_y + s\bar{\xi}_r^{xz} Z_0 \Delta z H_z \qquad (15)
\end{aligned}$$

where $s = j\,\omega$ is the Laplace parameter.

2) Maxwell–Faraday: One can follow the similar procedure by using Faraday–Maxwell's equation with the field sampling illustrated in Fig. 2.

Consider the x-component of the Maxwell–Faraday's curl equation in (2),

$$\begin{aligned}
&-\frac{\partial E_z}{\partial y} + \frac{\partial E_y}{\partial z} - J_{mx} \\
&\quad = \mu_0 \frac{\partial H_x}{\partial t} + \left(\sigma_m^{xx} * H_x + \sigma_m^{xy} * H_y + \sigma_m^{xz} * H_z\right) \\
&\qquad + \frac{\partial}{\partial t}\left[\frac{1}{c_0}\left(\zeta_r^{xx} * E_x + \zeta_r^{xy} * E_y + \zeta_r^{xz} * E_z\right) \right. \\
&\qquad\qquad \left. + \mu_0 \left(\chi_m^{xx} * H_x + \chi_m^{xy} * H_y + \chi_m^{xz} * H_z\right) \right]. \qquad (16)
\end{aligned}$$

$$\begin{aligned}
&\left[Z_0 \Delta z \left(H_{12}^z - H_1^z\right) + Z_0 \Delta y \left(H_2^y - H_9^y\right)\right]^{(n-1/2)} \\
&\quad = \frac{2}{\bar{C}_x}\Delta x \left[E_x^{(n)} - \tilde{E}_x^{(n-1/2)}\right] \\
&\qquad + Z_0 \frac{\Delta y \Delta z}{\Delta x}\left(\frac{\Delta x \sigma_e^{xx}}{\Delta x} * \Delta x E_x^{(n)} + \frac{\Delta x \sigma_e^{xy}}{\Delta y} * \Delta y E_y^{(n)} + \frac{\Delta x \sigma_e^{xz}}{\Delta z} * \Delta z E_z^{(n)} \right) + Z_0 \frac{\Delta y \Delta z}{\Delta x} \Delta x J_{ex}^{(n)} \\
&\qquad + \frac{\Delta t}{\bar{C}_x}\frac{\partial}{\partial t}\left[\begin{array}{l} \left(\frac{\Delta x \chi_e^{xx}}{\Delta x} * \Delta x E_x^{(n)} + \frac{\Delta x \chi_e^{xy}}{\Delta y} * \Delta y E_y^{(n)} + \frac{\Delta x \chi_e^{xz}}{\Delta z} * \Delta z E_z^{(n)} \right) \\ + \left(\frac{\Delta x \xi_r^{xx}}{\Delta x} * Z_0 \Delta x H_x^{(n)} + \frac{\Delta x \xi_r^{xy}}{\Delta y} * Z_0 \Delta y H_y^{(n)} + \frac{\Delta x \xi_r^{xz}}{\Delta z} * Z_0 \Delta z H_z^{(n)} \right) \end{array} \right]
\end{aligned} \qquad (9)$$

$$\begin{aligned}
\left[\Delta x E_x^{(n)}\right]_r &= \Delta x E_x^{(n)} + \bar{\sigma}_e^{xx} * \Delta x E_x^{(n)} + \bar{\sigma}_e^{xy} * \Delta y E_y^{(n)} + \bar{\sigma}_e^{xz} * \Delta z E_z^{(n)} \\
&\quad + \frac{\partial}{\partial t}\left[\begin{array}{l} \left(\bar{\chi}_e^{xx} * \Delta x E_x^{(n)} + \bar{\chi}_e^{xy} * \Delta y E_y^{(n)} + \bar{\chi}_e^{xz} * \Delta z E_z^{(n)} \right) \\ + \left(\bar{\xi}_r^{xx} * Z_0 \Delta x H_x^{(n)} + \bar{\xi}_r^{xy} * Z_0 \Delta y H_y^{(n)} + \bar{\xi}_r^{xz} * Z_0 \Delta z H_z^{(n)} \right) \end{array} \right] \qquad (14)
\end{aligned}$$

According to the illustration shown in Fig. 2, (16) can be sampled in the plane yOz, as shown in (17) at the bottom of this page.

Now, by setting

$$\tilde{H}_x = \frac{H_4^x + H_8^x + H_5^x + H_7^x + \hat{Z}_{sx} H_{16}^x}{4 + \hat{Z}_{sx}} \tag{18}$$

$$\hat{Z}_{sx} = 4\left(\frac{\Delta y \Delta z}{s\Delta x} - 1\right) = \frac{2}{\bar{D}_x} - 4 \tag{19}$$

$$\bar{D}_x = \frac{s\Delta x}{2\Delta y \Delta z} = \bar{C}_x. \tag{20}$$

Equation (17) can be written as (21), shown at the bottom of this page.

After manipulation, (21) gives (22), shown at the bottom of this page.

By setting

$$\bar{\sigma}_m^{ij} = \frac{\Delta k \Delta j}{2 Z_0 \Delta i} \bar{D}_i \frac{\Delta i}{\Delta j} \sigma_m^{ij} \tag{23}$$

$$\bar{\chi}_m^{ij} = \frac{\Delta t \Delta i}{2\Delta j} \chi_m^{ij} \text{ and } \bar{\zeta}_r^{ij} = \frac{\Delta t \Delta i}{2\Delta j} \zeta_r^{ij} \tag{24}$$

$$\begin{aligned}
\left[Z_0 \Delta x H_x^{(n)}\right]_{\text{source}} &= -\frac{\Delta z \Delta y}{2 Z_0 \Delta x} \bar{D}_x Z_0 \Delta x J_{mx}^{(n)} \\
\left[Z_0 \Delta x H_x^{(n)}\right]_{\text{nor}} &= \bar{D}_x (a_5 - a_7 - a_4 + a_8 + \hat{Z}_{sx} a_{16}) \\
\left[Z_0 \Delta x H_x^{(n)}\right]_{\text{nor}} &+ \left[Z_0 \Delta x H_x^{(n)}\right]_{\text{source}} \\
&= \left[Z_0 \Delta x H_x^{(n)}\right]_r .
\end{aligned} \tag{25}$$

Equation (22) becomes (26), shown at the bottom of the following page.

Applying the Laplace transform eliminates the convolution products, and (26) can be written in the compact form

$$\begin{aligned}
[Z_0 \Delta x H_x]_r = {} & Z_0 \Delta x H_x \left(1 + \bar{\sigma}_m^{xx} + s\bar{\chi}_m^{xx}\right) \\
& + Z_0 \Delta y H_y \left(\bar{\sigma}_m^{xy} + s\bar{\chi}_m^{xy}\right) \\
& + Z_0 \Delta z H_z \left(\bar{\sigma}_m^{xz} + s\bar{\chi}_m^{xz}\right) \\
& + s\left(\bar{\zeta}_r^{xx} \Delta x E_x + \bar{\zeta}_r^{xy} \Delta y E_y + \bar{\zeta}_r^{xz} \Delta z E_z\right).
\end{aligned} \tag{27}$$

$$\begin{aligned}
&\left[-\Delta z \left(E_7^z - E_5^z\right) + \Delta y \left(E_8^y - E_4^y\right)\right]^{(n-1/2)} \\
&= \frac{4\Delta z \Delta y}{s\Delta x} Z_0 \Delta x \left[H_x^{(n)} - \tilde{H}_x^{(n-1/2)}\right] \\
&\quad + \frac{\Delta z \Delta y}{Z_0} \left(\frac{\sigma_m^{xx}}{\Delta x} * Z_0 \Delta x H_x^{(n)} + \frac{\sigma_m^{xy}}{\Delta y} * Z_0 \Delta y H_y^{(n)} + \frac{\sigma_m^{xz}}{\Delta z} * Z_0 \Delta z H_z^{(n)}\right) + \Delta z \Delta y J_{mx}^{(n)} \\
&\quad + \frac{\Delta z \Delta y}{c_0} \frac{\partial}{\partial t} \left[\begin{array}{l} \left(\frac{\chi_m^{xx}}{\Delta x} * Z_0 \Delta x H_x^{(n)} + \frac{\chi_m^{xy}}{\Delta y} * Z_0 \Delta y H_y^{(n)} + \frac{\chi_m^{xz}}{\Delta z} * Z_0 \Delta z H_z^{(n)}\right) \\ \quad + \left(\frac{\zeta_r^{xx}}{\Delta x} * \Delta x E_x^{(n)} + \frac{\zeta_r^{xy}}{\Delta y} * \Delta y E_y^{(n)} + \frac{\zeta_r^{xz}}{\Delta z} * \Delta z E_z^{(n)}\right) \end{array}\right]
\end{aligned} \tag{17}$$

$$\begin{aligned}
&\left[-\Delta z \left(E_7^z - E_5^z\right) + \Delta y \left(E_8^y - E_4^y\right)\right]^{(n-1/2)} \\
&= \frac{2}{\bar{D}_x} Z_0 \Delta x \left[H_x^{(n)} - \tilde{H}_x^{(n-1/2)}\right] \\
&\quad + \frac{\Delta z \Delta y}{Z_0 \Delta x} \left(\frac{\Delta x \sigma_m^{xx}}{\Delta x} * Z_0 \Delta x H_x^{(n)} + \frac{\Delta x \sigma_m^{xy}}{\Delta y} * Z_0 \Delta y H_y^{(n)} + \frac{\Delta x \sigma_m^{xz}}{\Delta z} * Z_0 \Delta z H_z^{(n)}\right) \\
&\quad + \frac{\Delta z \Delta y}{Z_0 \Delta x} Z_0 \Delta x J_{mx}^{(n)} + \frac{\Delta t}{\bar{D}_x} \frac{\partial}{\partial t} \left[\begin{array}{l} \left(\frac{\Delta x \chi_m^{xx}}{\Delta x} * Z_0 \Delta x H_x^{(n)} + \frac{\Delta x \chi_m^{xy}}{\Delta y} * Z_0 \Delta y H_y^{(n)} + \frac{\Delta x \chi_m^{xz}}{\Delta z} * Z_0 \Delta z H_z^{(n)}\right) \\ + \left(\frac{\Delta x \zeta_r^{xx}}{\Delta x} * \Delta x E_x^{(n)} + \frac{\Delta x \zeta_r^{xy}}{\Delta y} * \Delta y E_y^{(n)} + \frac{\Delta x \zeta_r^{xz}}{\Delta z} * \Delta z E_z^{(n)}\right) \end{array}\right]
\end{aligned} \tag{21}$$

$$\begin{aligned}
&\bar{D}_x (a_5 - a_7 - a_4 + a_8 + \hat{Z}_{sx} a_{16}) \\
&= Z_0 \Delta x H_x^{(n)} \\
&\quad + \frac{\Delta z \Delta y}{2 Z_0 \Delta x} \bar{D}_x \left(\frac{\Delta x \sigma_m^{xx}}{\Delta x} * Z_0 \Delta x H_x^{(n)} + \frac{\Delta x \sigma_m^{xy}}{\Delta y} * Z_0 \Delta y H_y^{(n)} + \frac{\Delta x \sigma_m^{xz}}{\Delta z} * Z_0 \Delta z H_z^{(n)}\right) + \frac{\Delta z \Delta y}{2 Z_0 \Delta x} \bar{D}_x Z_0 \Delta x J_{mx}^{(n)} \\
&\quad + \frac{\Delta t}{2} \frac{\partial}{\partial t} \left[\begin{array}{l} \left(\frac{\Delta x \chi_m^{xx}}{\Delta x} * Z_0 \Delta x H_x^{(n)} + \frac{\Delta x \chi_m^{xy}}{\Delta y} * Z_0 \Delta y H_y^{(n)} + \frac{\Delta x \chi_m^{xz}}{\Delta z} * Z_0 \Delta z H_z^{(n)}\right) \\ + \left(\frac{\Delta x \zeta_r^{xx}}{\Delta x} * \Delta x E_x^{(n)} + \frac{\Delta x \zeta_r^{xy}}{\Delta y} * \Delta y E_y^{(n)} + \frac{\Delta x \zeta_r^{xz}}{\Delta z} * \Delta z E_z^{(n)}\right) \end{array}\right]
\end{aligned} \tag{22}$$

In compact matrix notation, the process can be written as follows:

$$\begin{bmatrix} \Delta x E_x \\ \Delta y E_y \\ \Delta z E_z \\ Z_0 \Delta x H_x \\ Z_0 \Delta y H_y \\ Z_0 \Delta z H_z \end{bmatrix}_r = ([I_d] + [\sigma] + s[M]) \begin{bmatrix} \Delta x E_x \\ \Delta y E_y \\ \Delta z E_z \\ Z_0 \Delta x H_x \\ Z_0 \Delta y H_y \\ Z_0 \Delta z H_z \end{bmatrix} \tag{28}$$

with $[I_d]$ being the identity matrix, and where

$$[\sigma] = \begin{bmatrix} \bar{\sigma}_e^{xx} & \bar{\sigma}_e^{xy} & \bar{\sigma}_e^{xz} & & & \\ \bar{\sigma}_e^{yx} & \bar{\sigma}_e^{yy} & \bar{\sigma}_e^{yz} & & 0 & \\ \bar{\sigma}_e^{zx} & \bar{\sigma}_e^{zy} & \bar{\sigma}_e^{zz} & & & \\ & & & \bar{\sigma}_m^{xx} & \bar{\sigma}_m^{xy} & \bar{\sigma}_m^{xz} \\ & 0 & & \bar{\sigma}_m^{yx} & \bar{\sigma}_m^{yy} & \bar{\sigma}_m^{yz} \\ & & & \bar{\sigma}_m^{zx} & \bar{\sigma}_m^{zy} & \bar{\sigma}_m^{zz} \end{bmatrix} \tag{29}$$

and

$$[M] = \begin{bmatrix} \bar{\chi}_e^{xx} & \bar{\chi}_e^{xy} & \bar{\chi}_e^{xz} & \bar{\xi}_r^{xx} & \bar{\xi}_r^{xy} & \bar{\xi}_r^{xz} \\ \bar{\chi}_e^{yx} & \bar{\chi}_e^{yy} & \bar{\chi}_e^{yz} & \bar{\xi}_r^{yx} & \bar{\xi}_r^{yy} & \bar{\xi}_r^{yz} \\ \bar{\chi}_e^{zx} & \bar{\chi}_e^{zy} & \bar{\chi}_e^{zz} & \bar{\xi}_r^{zx} & \bar{\xi}_r^{zy} & \bar{\xi}_r^{zz} \\ \bar{\zeta}_r^{xx} & \bar{\zeta}_r^{xy} & \bar{\zeta}_r^{xz} & \bar{\chi}_m^{xx} & \bar{\chi}_m^{xy} & \bar{\chi}_m^{xz} \\ \bar{\zeta}_r^{yx} & \bar{\zeta}_r^{yy} & \bar{\zeta}_r^{yz} & \bar{\chi}_m^{yx} & \bar{\chi}_m^{yy} & \bar{\chi}_m^{yz} \\ \bar{\zeta}_r^{zx} & \bar{\zeta}_r^{zy} & \bar{\zeta}_r^{zz} & \bar{\chi}_m^{zx} & \bar{\chi}_m^{zy} & \bar{\chi}_m^{zz} \end{bmatrix}. \tag{30}$$

Hence, the right-hand-side vector of (28) gives the updated value of all field components at the node center and time n by inverting the matrix such as (31), shown at the bottom of this page. One defines the tensor

$$[t] = ([I_d] + [\sigma] + s[M])^{-1}. \tag{32}$$

Usually, elements of (32) are complex valued expressions and approaches such as Prony's decomposition should be used.

One now has all quantities to compute updated field values at the node center through the use of the$z$-transform to obtain $[t]^{-1}$in time domain

$$\begin{bmatrix} E_x \\ E_y \\ E_z \\ H_x \\ H_y \\ Hz \end{bmatrix}_{\text{up}} = [t]^{-1}_{\text{material}} \otimes \begin{bmatrix} E_x \\ E_y \\ E_z \\ H_x \\ H_y \\ Hz \end{bmatrix}_r. \tag{33}$$

Once the discrete-time system is characterized, one can determine the *updated* fields in the node arms for the next time iteration. Note that, in this formulation, these quantities are defined as *updated* to distinguish them from the reflected voltages on the transmission lines. In previous formulations [6]–[8], these quantities are called the reflected fields.

B. Digital Filtering

Once elements of the tensor (32) are determined, it is necessary to transform it to the discrete time domain to make it compatible with the TLM algorithm. This is achieved by using the$z$-transform. However, tensor's element expressions have to be first approximated by polynomial ratios expressed in frequency domain.

1) Frequency-Domain Prony Method: Given a set of NF complex frequency-domain data samples, $\{F_0, F_1, F_2, \ldots, F_{\text{NF}-1}\}$, Prony's method [10], [11] yields a least square approximation by using exponential basis functions. Let NP be the number of poles,C_i be the residue,

$$\begin{aligned} \left[Z_0 \Delta x H_x^{(n)}\right]_r = Z_0 \Delta x H_x^{(n)} + \left(\bar{\sigma}_m^{xx} * Z_0 \Delta x H_x^{(n)} + \bar{\sigma}_m^{xy} * Z_0 \Delta y H_y^{(n)} + \bar{\sigma}_m^{xz} * Z_0 \Delta z H_z^{(n)}\right) \\ + \frac{\partial}{\partial t} \left[\begin{array}{l} \left(\bar{\chi}_m^{xx} * Z_0 \Delta x H_x^{(n)} + \bar{\chi}_m^{xy} * Z_0 \Delta y H_y^{(n)} + \bar{\chi}_m^{xz} * Z_0 \Delta z H_z^{(n)}\right) \\ + \left(\bar{\zeta}_r^{xx} * \Delta x E_x^{(n)} + \bar{\zeta}_r^{xy} * \Delta y E_y^{(n)} + \bar{\zeta}_r^{xz} * \Delta z E_z^{(n)}\right) \end{array} \right] \end{aligned} \tag{26}$$

$$\begin{aligned} &\begin{bmatrix} \Delta x E_x \\ \Delta y E_y \\ \Delta z E_z \\ Z_0 \Delta x H_x \\ Z_0 \Delta y H_y \\ Z_0 \Delta z H_z \end{bmatrix}_r \\ &= \begin{bmatrix} 1 + \bar{\sigma}_e^{xx} + s\bar{\chi}_e^{xx} & \bar{\sigma}_e^{xy} + s\bar{\chi}_e^{xy} & \bar{\sigma}_e^{xz} + s\bar{\chi}_e^{xz} & s\bar{\xi}_r^{xx} & s\bar{\xi}_r^{xy} & s\bar{\xi}_r^{xz} \\ \bar{\sigma}_e^{yx} + s\bar{\chi}_e^{yx} & 1 + \bar{\sigma}_e^{yy} + s\bar{\chi}_e^{yy} & \bar{\sigma}_e^{yz} + s\bar{\chi}_e^{yz} & s\bar{\xi}_r^{yx} & s\bar{\xi}_r^{yy} & s\bar{\xi}_r^{yz} \\ 1 + \bar{\sigma}_e^{zx} + s\bar{\chi}_e^{zx} & \bar{\sigma}_e^{zy} + s\bar{\chi}_e^{zy} & 1 + \bar{\sigma}_e^{zz} + s\bar{\chi}_e^{zz} & s\bar{\xi}_r^{zx} & s\bar{\xi}_r^{zy} & s\bar{\xi}_r^{zz} \\ s\bar{\zeta}_r^{xx} & s\bar{\zeta}_r^{xy} & s\bar{\zeta}_r^{xz} & 1 + \bar{\sigma}_m^{xx} + s\bar{\chi}_m^{xx} & \bar{\sigma}_m^{xy} + s\bar{\chi}_m^{xy} & \bar{\sigma}_m^{xz} + s\bar{\chi}_m^{xz} \\ s\bar{\zeta}_r^{yx} & s\bar{\zeta}_r^{yy} & s\bar{\zeta}_r^{yz} & \bar{\sigma}_m^{yx} + s\bar{\chi}_m^{yx} & 1 + \bar{\sigma}_m^{yy} + s\bar{\chi}_m^{yy} & \bar{\sigma}_m^{yz} + s\bar{\chi}_m^{yz} \\ s\bar{\zeta}_r^{zx} & s\bar{\zeta}_r^{zy} & s\bar{\zeta}_r^{zz} & \bar{\sigma}_m^{zx} + s\bar{\chi}_m^{zx} & \bar{\sigma}_m^{zy} + s\bar{\chi}_m^{zy} & 1 + \bar{\sigma}_m^{zz} + s\bar{\chi}_m^{zz} \end{bmatrix} \\ &\times \begin{bmatrix} \Delta x E_x \\ \Delta y E_y \\ \Delta z E_z \\ Z_0 \Delta x H_x \\ Z_0 \Delta y H_y \\ Z_0 \Delta z H_z \end{bmatrix} \end{aligned} \tag{31}$$

and s_{pi} be the complex frequency of the$i$th pole, the starting point for this procedure is the approximation

$$f(t) = \sum_{i=0}^{\mathrm{NP}-1} C_i e^{s_{pi}t}. \tag{34}$$

Taking the Laplace transform yields

$$F(s) = \sum_{i=0}^{\mathrm{NP}-1} \frac{C_i}{s - s_{pi}} = \frac{\sum_{i=0}^{\mathrm{NP}-1} b_i s^i}{\sum_{i=0}^{\mathrm{NP}} a_i s^i}. \tag{35}$$

Equation (35) is modified by increasing the order of the numerator by one for physical reasons. The goal of the Prony method is to identify the Padé coefficients a's and b's.

After applying the procedure detailed in [12] to solve (35), Padé coefficients can be determined. Solving for the roots of the numerator and denominator lead to

$$\begin{aligned} F(s) &= \frac{b_{\mathrm{NP}} \prod_{i=0}^{\mathrm{NP}-1} (s - s_{zi})}{\prod_{i=0}^{\mathrm{NP}-1} (s - s_{pi})} \\ &= \frac{b_{\mathrm{NP}}(s-s_{z0})(s-s_{z1})(s-s_{z2}) \ldots \left(s-s_{z(\mathrm{NP}-1)}\right)}{(s-s_{p0})(s-s_{p1})(s-s_{p2}) \ldots (s-s_{p(\mathrm{NP}-1)})}. \end{aligned} \tag{36}$$

2) Z-Transform Method: Once the approximation has been obtained as expressed in (36), the discrete-time model is developed by using the z-transform technique. The bilinear z-transform for a single zero is

$$(s - s_{zi}) \xrightarrow{Z} \alpha_{zi} \left(\frac{1 - z^{-1}\beta_{zi}}{1 + z^{-1}} \right). \tag{37}$$

where z is the time-shift operator and the z-domain zero is at

$$\alpha_{zi} = \frac{2 - s_{zi}\Delta t}{\Delta t} \text{ and } \beta_{zi} = \frac{2 + s_{zi}\Delta t}{2 - s_{zi}\Delta t}.$$

Applying (37) on (36) yields, after some manipulations,

$$\begin{aligned} F(z) &= \frac{\sum_{i=0}^{\mathrm{NP}} B_i z^{-i}}{\sum_{i=0}^{\mathrm{NP}} A_i z^{-i}} \\ &= \frac{B_0 + \sum_{i=1}^{\mathrm{NP}} B_i z^{-i}}{1 + \sum_{i=0}^{\mathrm{NP}} A_i z^{-i}} \\ &= B_0 + \frac{\sum_{i=1}^{\mathrm{NP}} B_i^{'} z^{-i}}{1 + \sum_{i=0}^{\mathrm{NP}} A_i z^{-i}} \end{aligned} \tag{38}$$

where

$$B_0 = b_{\mathrm{NP}} \prod_{i=0}^{\mathrm{NP}-1} \left(\frac{\alpha_{zi}}{\alpha_{pi}} \right),$$

$B_i^{'} = B_i - B_0 A_i$ and setting $A_0 = 1$.

3) State Space Equation: The transfer function that represents the reflectivity E_{up}/E_r can now be written in the following form:

$$E_{\mathrm{up}} = B_0 E_r + \frac{E_r \sum_{i=1}^{\mathrm{NP}} B_i^{'} z^{-i}}{1 + \sum_{i=0}^{\mathrm{NP}} A_i z^{-i}}. \tag{39}$$

The output equation of the state-space system is

$$E_{\mathrm{up}} = B_0 E_r + \sum_{i=1}^{\mathrm{NP}} B_i^{'} X_i \tag{40}$$

where X_i are the state variables. Combining (39) and (40) yields the state equation

$$E_r \sum_{i=1}^{\mathrm{NP}} \frac{B_i^{'} z^{-i}}{1 + \sum_{i=0}^{\mathrm{NP}} A_i z^{-i}} = \sum_{i=1}^{\mathrm{NP}} B_i^{'} X_i. \tag{41}$$

Evaluation of this expression for each variable leads to

$$X_1 = z^{-1} E_r - z^{-1} \sum_{i=1}^{\mathrm{NP}} A_i X_i \tag{42}$$

$$X_2 = z^{-1} X_1 \tag{43}$$

$$X_3 = -z^{-1} X_2, \ldots, X_{\mathrm{NP}} = z^{-1} X_{\mathrm{NP}-1}. \tag{44}$$

Expressing (42) and (44) in matrix form yields

$$E_{\mathrm{up}} = B_0 E_r + \begin{bmatrix} B_1^{'} & B_2^{'} & B_3^{'} & \cdots & B_{\mathrm{NP}}^{'} \end{bmatrix} \begin{bmatrix} X_1 \\ X_2 \\ X_3 \\ \vdots \\ X_{\mathrm{NP}} \end{bmatrix} \tag{45}$$

and

$$\begin{aligned} &\begin{bmatrix} X_1 \\ X_2 \\ X_3 \\ \vdots \\ X_{\mathrm{NP}} \end{bmatrix} \\ &= z^{-1} \begin{bmatrix} -A_1 & -A_2 & -A_3 & \ldots & -A_{\mathrm{NP}-1} & -A_{\mathrm{NP}} \\ 1 & & & & & \\ & 1 & & & & \\ & & 1 & & & \\ & & & \ddots & & \\ & & & & 1 & \end{bmatrix} \\ &\quad \times \begin{bmatrix} X_1 \\ X_2 \\ X_3 \\ \vdots \\ X_{\mathrm{NP}} \end{bmatrix} + z^{-1} \begin{bmatrix} 1 \\ 0 \\ 0 \\ \vdots \\ 0 \end{bmatrix} E_r. \end{aligned} \tag{46}$$

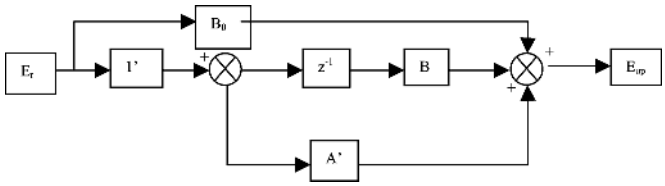

Fig. 3. Representation of the state space equations.

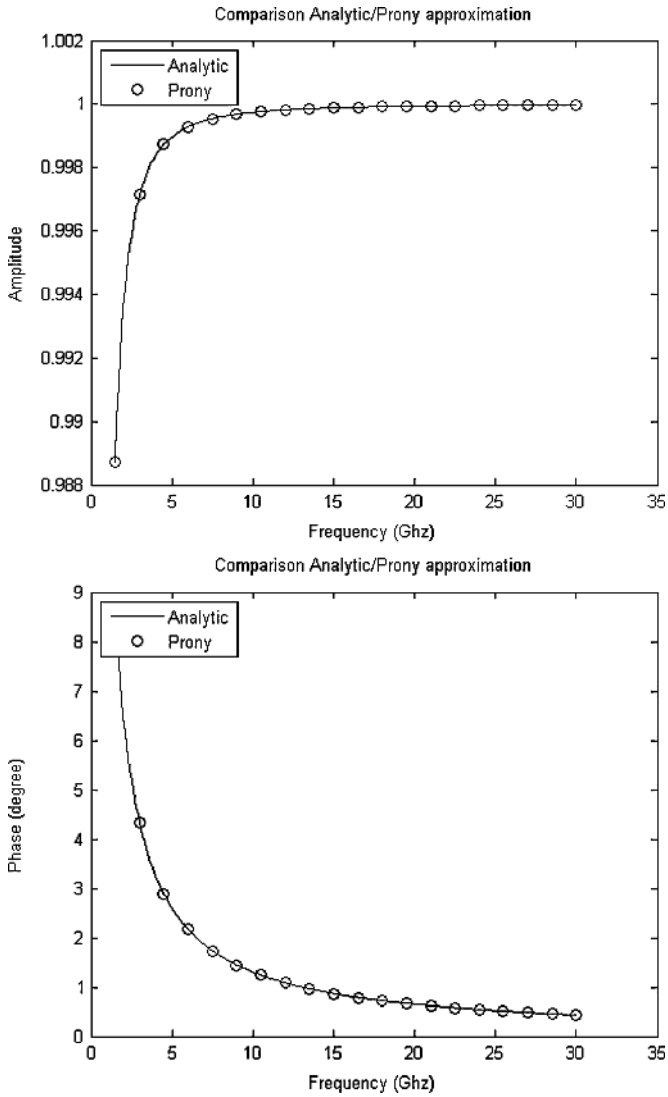

Fig. 4. Prony approximation of the tensor element (amplitude and phase).

Using compact notation, the general system of these equations is

$$E_{\text{up}} = B_0 E_r + B_i^{'} X$$
$$X = z^{-1} A^{'} X + z^{-1} 1^{'} E_r \tag{47}$$

The flow graph shown in Fig. 3 illustrates the general state space system corresponding to (47).

III. Anisotropic and Dispersive Media

To demonstrate the novelty and relevance of the proposed technique, two different types of dispersive and anisotropic materials are studied: an unmagnetized plasma considered as a dispersive medium and a nonsaturated ferrite (with an arbitrary magnetization state) characterized by an anisotropic and dispersive extra diagonal tensor.

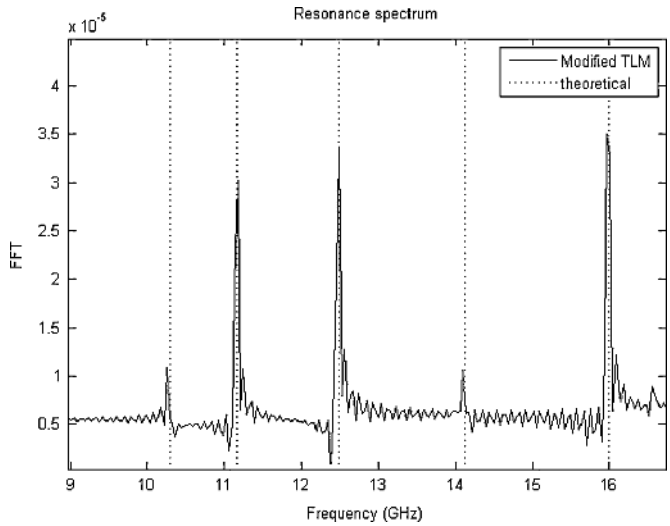

Fig. 5. Plasma-filled metal cavity resonance spectrum. Vertical lines show theoretical solutions.

TABLE II
Comparison Between TLM and Theoretical Results

Resonance Modes	Theoretical Resonance Frequencies of the cavity [GHz]	Simulated Resonance Frequencies of the cavity [GHz]	Relative Error [%]
101	10.2915	10.2698	0.210
102	11.1653	11.1608	0.040
103	12.4865	12.4893	0.022
104	14.1302	14.1008	0.208
105	15.9973	15.9867	0.066

A. Isotropic and Dispersive Media

One can consider an unmagnetized plasma with the following electric susceptibility:

$$\chi_e = \varepsilon_p - 1 = \begin{pmatrix} \kappa_p & 0 & 0 \\ 0 & \kappa_p & 0 \\ 0 & 0 & \kappa_p \end{pmatrix} - [I_d] \tag{48}$$

where $\kappa_p = 1 - (\omega_p^2)/(\omega(\omega - j\nu_p))$, ω_p is the plasma pulsation resonance and ν_p is the plasma collision frequency.

The plasma is considered as a dispersive dielectric with no conductivity $\sigma = 0$. Equating (48) and (32) gives the resulting tensor

$$[t]_{\text{plasma}} = \begin{pmatrix} 1 + s \cdot \chi_e & 0 & & \dots & 0 \\ 0 & 1 + s \cdot \chi_e & & & \\ & & 1 + s \cdot \chi_e & & \vdots \\ \vdots & & & 1 & \\ & & & & 1 \quad 0 \\ 0 & & \dots & & 0 \quad 1 \end{pmatrix}^{-1}. \tag{49}$$

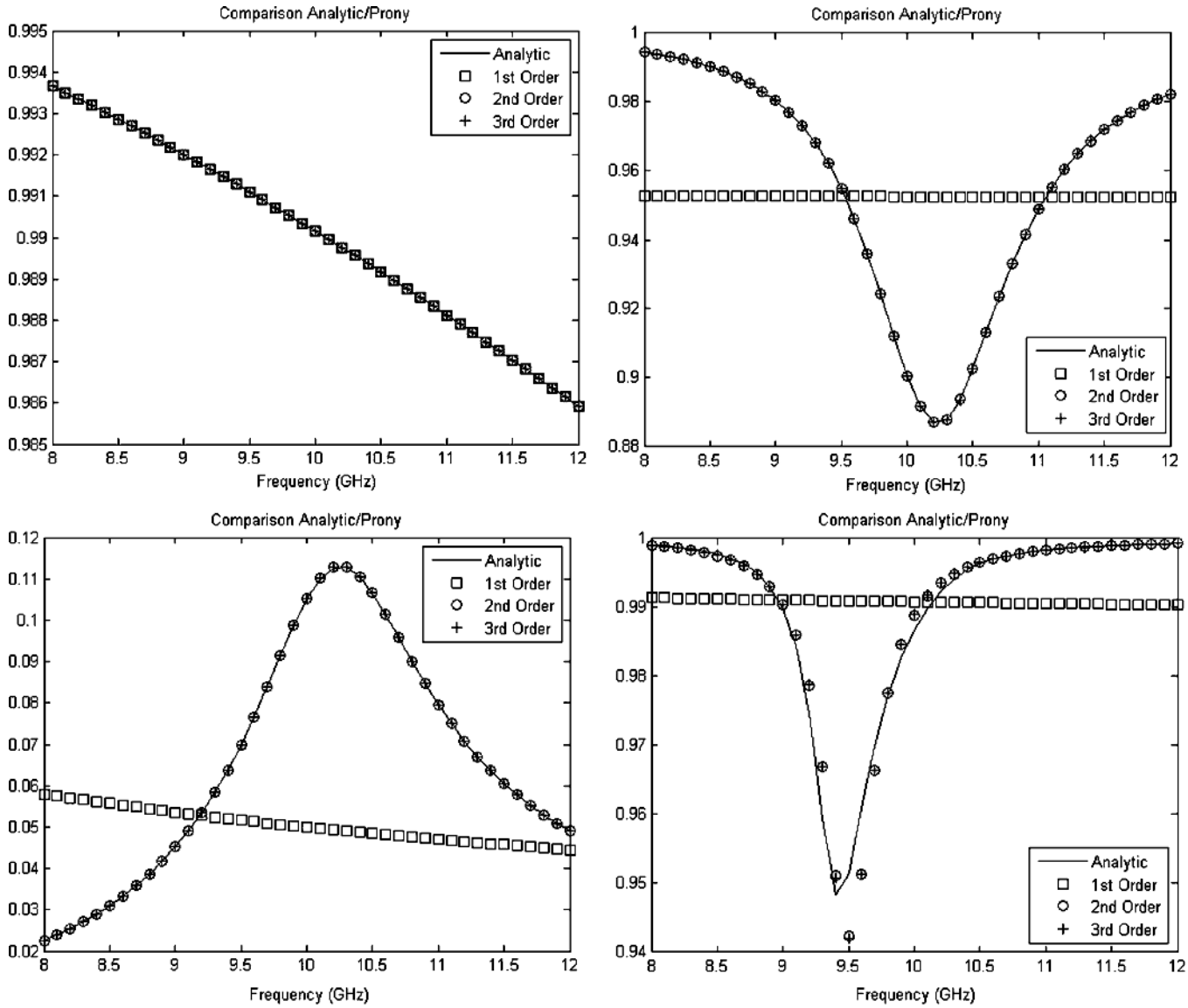

Fig. 6. Prony approximation of tensor's elements (absolute values of f_1, f_2, f_3, and f_4).

The inverse matrix is given by inverting each diagonal element

$$[t]^{-1}_{\text{plasma}} = \begin{pmatrix} \frac{1}{1+s\cdot\chi_e} & 0 & & \dots & 0 \\ 0 & \frac{1}{1+s\cdot\chi_e} & & & \\ & & \frac{1}{1+s\cdot\chi_e} & & \vdots \\ \vdots & & & 1 & \\ & & & & 1 \quad 0 \\ 0 & & \dots & & 0 \quad 1 \end{pmatrix}. \tag{50}$$

The element of the tensor is estimated using the frequency-domain Prony method. Starting with the function known analytically in the frequency domain, which is, in this case, each element of the tensor $[t]^{-1}$,

$$f(s) = \frac{1}{1+s\cdot\chi_e}. \tag{51}$$

Note that this is a first-order function.

By applying Prony's decomposition, the approximation of the function $f(s)$ is then performed. Fig. 4(a) shows a comparison of the analytic and approximated amplitude function. The Prony approximation also gives a very good fit of the phase of the function, as shown in Fig. 4(b).

Finally, a digital filtering is performed by applying a z-transformation to obtain (33) in time domain. as described in Section II.

The studied plasma sample has the following characteristics:

$$\omega_p = 4140 * 10^7 \text{ rad/s} \quad \nu_p = 1 \text{ GHz}.$$

The medium fills a rectangular metal cavity and resonance frequencies have to be determined. One of the dimensions (along the height) is small so that only TE_{m0p} modes are excited. The cavity is excited by a Gaussian pulse and a fast Fourier transform (FFT) is performed to determine mode resonance frequencies.

Fig. 5 shows the mode spectrum, and resonance frequencies are compared with theoretical results. As can be observed in

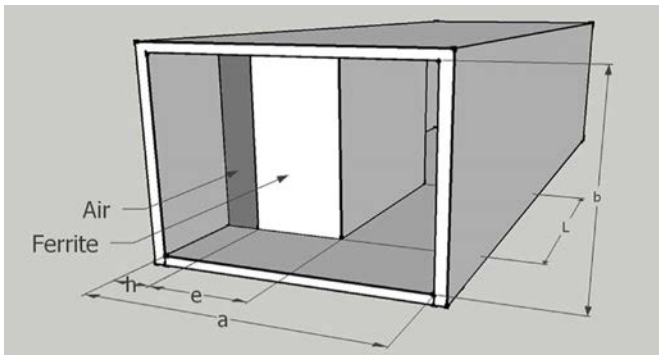

Fig. 7. Rectangular waveguide measurement cell.

Table II, comparison between both methods yields some excellent agreement.

B. Anisotropic and Dispersive Magnetic Media

Depending on the strength of the applied magnetic dc field, a ferrite medium can be set in various states of magnetization: completely demagnetized, fully saturated [3], remanent, or partially saturated [13]–[15]. In the latter case, the ferrite is subdivided into Weiss domains, and thus must be considered as heterogeneous medium. This makes the calculation of the tensor quite complicated. To circumvent this difficulty, empirical models of permeability tensor were proposed [15], [16]. These models have the disadvantage of not presenting all the elements of the permeability tensor in a single course. That is why a new statistic model that provides all the elements of the tensor of ferrites in a single calculation process and that takes the hysteresis phenomenon into account was needed.

The permeability tensor model developed in our laboratory [4], [17] has the advantage, compared to theoretical approaches previously proposed in the literature, of not considering the partly magnetized medium as composed of independent domains, but rather made of interactive grains composed of coupling domains.

Assuming that a dc magnetic field is applied along the y-direction, the permeability tensor in the Cartesian coordinate system takes the following well-known form:

$$\overleftrightarrow{\mu} = \mu_0 \begin{pmatrix} \mu & 0 & -j\kappa \\ 0 & \mu_y & 0 \\ j\kappa & 0 & \mu \end{pmatrix} \tag{52}$$

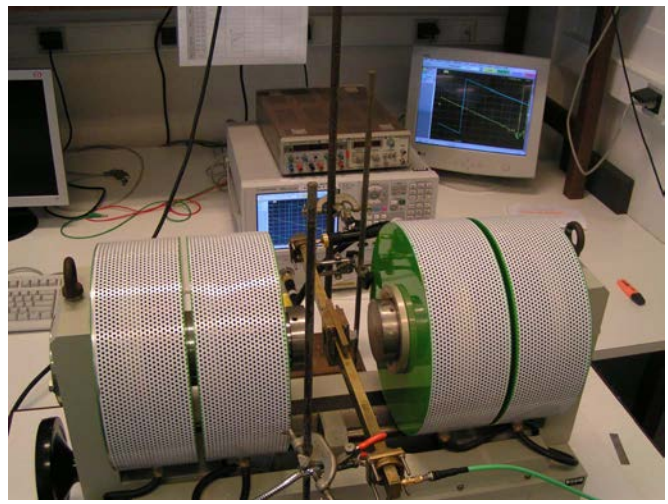

Fig. 8. Experimental test device.

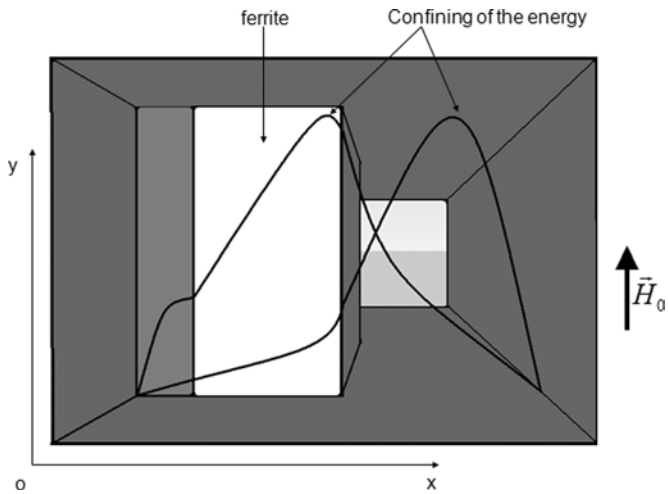

Fig. 9. Confining of the energy along the x-axis in the waveguide cross section: waves propagated in the positive and negative directions.

where all tensor components $\mu = \mu^{'} - j\mu^{''}, \kappa = \kappa^{'} - j\kappa^{''}$ and $\mu_y = \mu_y^{'} - j\mu_y^{''}$ in a real medium are complex quantities owing to the existence of magnetic losses. Equating (52) and (32) gives the resulting tensor shown in (53) at the bottom of the this page, where the electric susceptibility is related to its relative permittivity by $\chi_e = \varepsilon_r - 1$ and the magnetic susceptibility is $\chi_m = \overleftrightarrow{\mu}_r - 1$.

$$[t]_{\text{ferrite}} = \begin{pmatrix} \begin{pmatrix} 1+s\cdot\chi_e & & \\ & 1+s\cdot\chi_e & \\ & & 1+s\cdot\chi_e \end{pmatrix} & 0 \\ 0 & \begin{pmatrix} 1+s\cdot\chi_m & & -j\kappa\cdot s \\ & 1+s\cdot\chi_{my} & \\ j\kappa\cdot s & & 1+s.\chi_m \end{pmatrix} \end{pmatrix}^{-1} \tag{53}$$

$$[t]^{-1}_{\text{ferrite}} = \begin{pmatrix} \begin{pmatrix} f_1(s) & & \\ & f_1(s) & \\ & & f_1(s) \end{pmatrix} & 0 \\ 0 & \begin{pmatrix} f_2(s) & & f_3(s) \\ & f_4(s) & \\ -f_3(s) & & f_2(s) \end{pmatrix} \end{pmatrix} \tag{54}$$

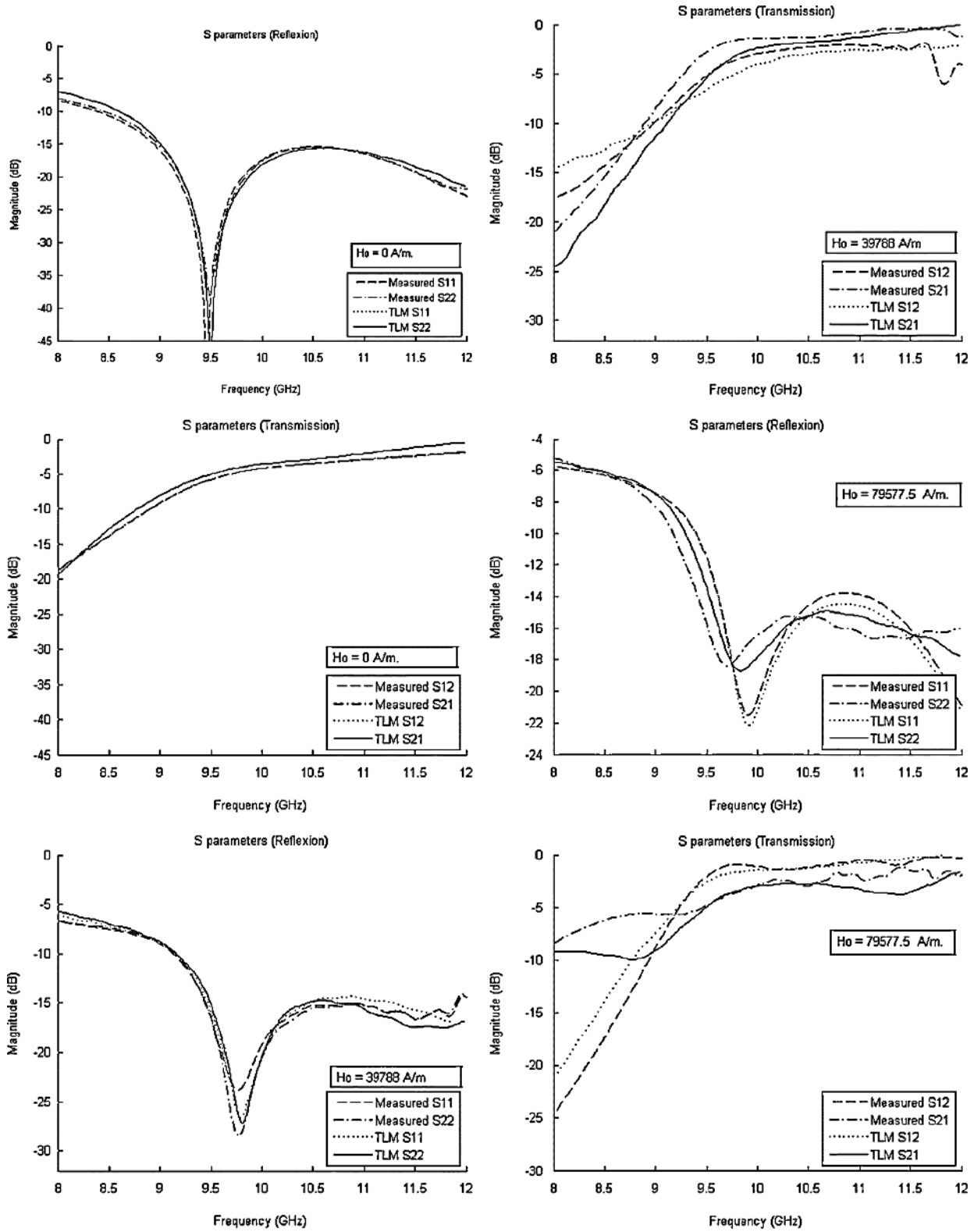

Fig. 10. S-parameters magnitude versus frequency for different values of the magnetic static field applied Ho. Ferrite under test properties: $4\pi Ms = 0.5$ T, $Ha = 15915$ A/m, $\Delta H = 39788$ A/m. (*top*) Magnetic static field applied $Ho = 0$ A/m. (*middle*) Magnetic static field applied $Ho = 39788$ A/m. (*bottom*) Magnetic static field applied.

One can write the inverse matrix as (54), shown at the bottom of the previous page, and where

$$f_1(s) = \frac{1}{1 + s \cdot \chi_e}$$

$$f_2(s) = \frac{1 + s.\chi_m}{(j\kappa \cdot s)^2 + (1 + s \cdot \chi_m)^2}$$

$$f_3(s) = \frac{j\kappa}{(j\kappa \cdot s)^2 + (1 + s \cdot \chi_m)^2}$$

$$f_4(s) = \frac{1}{1 + s \cdot \chi_{my}}.$$

Approximations of functions f_1, f_2, f_3, and f_4 are performed by applying Prony's decomposition with different values of NP. Fig. 6 shows that Prony's approximation gives an adequate fit to functions for $\mathrm{NP} \geq 2$. One can follow the same procedure detailed in Section II-B to perform the digital filtering for ferrites.

The above model is tested for validation by considering the reflection/transmission of a rectangular waveguide partly filled with ferrite, as shown in Fig. 7. The simulated S-parameters at X-band frequencies (8–12 GHz) will be compared with those measured for ferrites with well-known properties.

The experimental propagation structure is a waveguide loaded with ferrite that is positioned between the poles of an electromagnet to magnetize the sample as shown in Fig. 8.

When a uniform static magnetic field is applied along the side of the waveguide (y-axis of the Cartesian coordinate system), the field displacement occurs along the large side of the guide (x-axis) (Fig. 9). The nonreciprocity of the field displacement along the$y$-axis, which depends on the wave propagation direction, breaks the symmetry and the reciprocity of the cell. The condition of nonreciprocity of the cell has been proven by experimentation for different ferrites and values of the applied static field [19].

The validation of the proposed method consists in verifying that the S-parameters simulated with the TLM are in accordance with the ones measured for the ferrite biased by various strengths of the applied dc field.

The experimental results were obtained with an X-band rectangular waveguide (dimensions $a = 10.16$ and $b = 22.86$ mm) made of brass. S-parameters were measured for different values of the applied static magnetic field. The cell was loaded with a ferrite of a saturation magnetization $4\pi M_s = 0.5$ T, an anisotropy field $H_a = 15915.5$ A/m, and a resonance linewidth $\Delta H = 39788$ A/m.

The network analyzer (HP 8510B) calibration procedure, necessary to achieve accurate measurements at high frequencies, is a thru-reflect-line (TRL) [20].

Measurements illustrated in Fig. 10 proved the nonreciprocity of the measurement device. One can also observe a good agreement between the measurement and simulations over a wide frequency band and for different magnetization states of the ferrite. In the X-band, the theoretical and experimental S-parameters magnitudes are very close. Moreover, measurements and simulations show the same shift for the resonance frequency appearing in the reflection parameter.

The study of the cell sensitivity has allowed us to observe significant variations in the values and frequency behavior of S-parameters when the electromagnetic characteristics of the ferrite or the magnetic static field magnitude changes. This confirms the good accuracy of the theoretical results.

IV. Conclusion

The permeability tensor model of polycrystalline ferrites as a function of the dc bias field has been, for the first time, derived from a self-consistent theoretical approach and integrated in the TLM algorithm.

The TLM algorithm was implemented in the case of general anisotropic and dispersive media. The theoretical derivation was revisited, starting with Maxwell's equations, without invoking circuit analogy. The procedure is general and can be applied to derive the algorithm for extended TLM nodes.

Preliminary results computed in the case of a dispersive plasma medium show that the model is accurate when compared with theoretical results.

To illustrate the interest of this theoretical approach for practical applications, an example of a waveguide partly filled with a ferrite in different polarization states has been given. Comparison between experimental measurements and TLM simulations yielded a good agreement.

The ultimate objective is to insert a new pseudoanalytical model for ferrites in different magnetization states that are used for planar nonreciprocal devices implemented in low-temperature co-fired ceramic (LTCC).

References

[1] H. Mosallaei and K. Sarabandi, "Magneto-dielectrics in electromagnetics: Concept and applications," *IEEE Trans. Antennas Propag.*, vol. 52, no. 6, pp. 1558–1567, Jun. 2004.

[2] S. A. Oliver, P. Shi, W. Hu, H. How, S. W. McKnight, N. E. McGruer, P. M. Zavracky, and C. Vittoria, "Integrated self biased hexaferrite microstrip circulators for millimeter-wavelength applications," *IEEE Trans. Microw. Theory Tech.*, vol. 49, no. 2, pp. 385–387, Feb. 2001.

[3] D. Polder, "On the theory of ferromagnetic resonance," *Philosoph. Mag.*, vol. 40, pp. 99–115, Jan. 1949.

[4] P. Gelin and P. Quéffélec, "Generalized permeability tensor model: Application to barium hexaferrite in a remanent state for self-biased circulators," *IEEE Trans. Magn.*, vol. 44, no. 1, pp. 24–31, Jan. 2008.

[5] A. Guennou, B. Della, P. Quéffélec, P. Gelin, and J. L. Mattei, "Influence of the magnetic field nonuniformity on an X-band microstrip Y-junction circulator bandwidth: Theory/experiment comparison," *IEEE Trans. Magn.*, vol. 43, no. 6, pp. 2642–2644, Jun. 2007.

[6] J. Paul, C. Christopoulos, and D. Thomas, "Generalized material models in TLM—Part 1: Materials with frequency-dependent properties," *IEEE Trans. Antennas Propag.*, vol. 47, no. 10, pp. 1529–1534, Oct. 1999.

[7] J. Paul and C. Christopoulos, "Generalized material models in TLM\Part 2: Materials with frequency-dependent properties," *IEEE Trans. Antennas Propag.*, vol. 47, no. 10, pp. 1535–1542, Oct. 1999.

[8] J. Paul, C. Christopoulos, and D. Thomas, "Generalized material models in TLM—Part 3: Materials with nonlinear properties," *IEEE Trans. Antennas Propag.*, vol. 50, no. 7, pp. 997–1004, Jul. 2002.

[9] N. Peña and M. M. Ney, "A general formulation of a three-dimensional TLM condensed node with the modeling of electric and magnetic losses and current sources," in *12th Annu. Rev. Progr. Appl. Comput. Electromagn.*, Monterey, CA, Mar. 18–22, 1996, pp. 262–269.

[10] M. L. Van Blaricum and R. Mittra, "A technique for extracting the poles and residues of a system directly from its transient response," *IEEE Trans. Antennas Propag.*, vol. AP-23, no. 6, pp. 777–781, Nov. 1975.

[11] W. L. Ko and R. Mittra, "A combination of FDTD and Prony's methods for analyzing microwave integrated circuits," *IEEE Trans. Microw. Theory Tech.*, vol. 39, no. 12, pp. 2176–2181, Dec. 1991.

[12] J. N. Brittingharam, E. K. Miller, and J. L. Willows, "Pole extraction from real-frequency information," *Proc. IEEE*, vol. 68, no. 2, pp. 263–273, Feb. 1980.

[13] G. T. Rado, "Theory of the microwave permeability tensor and Faraday effect in non saturated ferromagnetic materials," *Phys. Rev.*, vol. 89, p. 529, 1953.

[14] E. Schlömann, "Microwave behavior of partially magnetized ferrites," *J. Appl. Phys.*, vol. 41, no. 1, pp. 204–214, Jan. 1970.

[15] J. Green and F. Sandy, "Microwave characterization of partially magnetized ferrites," *IEEE Trans. Microw. Theory Tech.*, vol. MTT-22, no. 6, pp. 641–645, Jun. 1974.

[16] M. Igarashi and Y. Nato, "Tensor permeability of partially magnetized ferrites," *IEEE Trans. Microw. Theory Tech.*, vol. MTT-13, no. 9, pp. 568–571, Sep. 1977.

[17] P. Gelin, P. Quéffélec, and F. Le Pennec, "Effect of domain and grain shapes on the dynamic behavior of polycristalline ferrites. Application to the initial permeability," *J. Appl. Phys.*, vol. 98, Sep. 2005, Art. ID 053906.

[18] P. Gelin and K. Berthou-Pichavant, "New consistent model for ferrite permeability tensor with arbitrary magnetization state," *IEEE Trans. Microw. Theory Tech.*, vol. 45, no. 8, pp. 1185–1192, Aug. 1997.
[19] P. Quéffélec, M. Le Floc'h, and Ph. Gelin, "Nonreciprocal cell for the broad band measurement of tensorial permeability of magnetized ferrites: Direct problem," *IEEE Trans. Microw. Theory Tech.*, vol. 47, no. 4, pp. 390–397, Apr. 1999.
[20] G. Engen and C. Hoer, "Thru-reflect-line: An improved technique for calibrating the dual six-port automatic network analyzer," *IEEE Trans. Microw. Theory Tech.*, vol. MTT-27, no. 12, pp. 987–993, Dec. 1979.